Deep-Blue Thermally Activated Delayed Fluorescence (TADF) Emitters for Light-Emitting Electrochemical Cells (LEECs)

Michael.Y. Wong,[a] *Maria-Grazia La-Placa,*[b] *Antonio Pertegas,*[b] *Henk J. Bolink*[b] *and Eli Zysman-Colman**[a]

[a] Organic Semiconductor Centre, EaStCHEM School of Chemistry, University of St Andrews, St Andrews, Fife, UK, KY16 9ST, Fax: +44-1334 463808; Tel: +44-1334 463826; E-mail: eli.zysman-colman@st-andrews.ac.uk; URL: http://www.zysman-colman.com

[b] Instituto de Ciencia Molecular (ICMol), Universidad de Valencia, Catedrático José Beltrán, 2, 46980 Paterna, Spain. E-mail: Henk.bolink@uv.es.

Abstract

Two deep blue thermally activated delayed fluorescence (TADF) emitters (**imCzDPS** and **imDPADPS**) that contain charged imidazolium groups tethered to the central luminophore were designed and synthesized as small molecule organic emitters for light-emitting electrochemical cell (LEEC) electroluminescent devices. The emission profile in doped thin films (5 wt% in PMMA) is very blue and narrow (λ_{PL}: 414 nm and 409 nm; full width at half maximum (FHWM): 62 nm and 46 nm for **imCzDPS** and **imDPADPS**, respectively) with good photoluminescence quantum efficiencies (Φ_{PL}: 44% and 49% for **imCzDPS** and **imDPADPS**, respectively). In neat films, emission maxima occur at 440 nm and 428 nm for **imCzDPS** and **imDPADPS**, respectively with comparable Φ_{PL} values of 44 and 61%, respectively. Both emitters

exhibit biexponential emission decay kinetics (nanosecond prompt and microsecond delayed fluorescence) in both MeCN solution and thin film, characteristic of TADF behaviour. While **imDPADPS** did not show any emission in the LEEC device, that of **imCzDPS** gave an electroluminescence (EL) maximum at 470 nm and CIE coordinates of (0.208, 0.250), which makes this device amongst the bluest reported to date. However, the maximum device luminance achieved was 2.5 cd m^{-2} and this poor brightness was attributed to the electrochemical instability of the emitter in LEEC architecture, as evidenced by the additional peak around 550 nm observed in the EL spectrum.

Introduction

Twenty per cent of World electricity consumption is devoted to lighting.[1] A vast effort has been dedicated to developing low-energy lighting technology in part to meet greenhouse gas emission targets and reduce global energy demands. Organic light-emitting diode (OLED) devices are a lighting technology that possesses great promise due in part to their lower operating voltages and wide range of accessible colours, including white light emission. One major bottleneck for high OLED efficiency is the challenge in utilizing all the excitons electrically generated in the device upon hole and electron recombination, which, according to spin statistics, constitute 25% singlet and 75% triplet excitons.[2] OLEDs using fluorophores in the emitting layer can only harvest the singlet excitons to produce light while the triplet excitons dissipate their energies to the surrounding as heat.[3] When limitations in light outcoupling are taken into account, the maximum external quantum efficiency (EQE) is limited to 5%. To overcome this limitation in device efficiency, phosphorescent

organometallic complexes were developed. The presence of the heavy metal centre promotes strong intersystem crossing (ISC), the result of which is that in the device both singlet and triplet excitons contribute to light emission.[4] However, these complexes are made using expensive and rare metals such as iridium and platinum, which inevitably will hinder their large-scale use and render them price uncompetitive for a replacement lighting technology, particularly in the developing world. Recently, small molecule thermally activated delayed fluorescence (TADF) emitters, which are likewise capable of converting up to 100% of the excitons in the device into light, have come to the fore as a viable alternative to the present state-of-the-art phosphorescent emitters.[5] The operational mechanism underpinning TADF relies on a small energy difference (ΔE_{ST}) between the lowest singlet state (S_1) and lowest triplet state (T_1), which enables triplet excitons to be thermally up-converted to emissive singlet excitons by reverse intersystem-crossing (RISC).[6] Recent examples of emitters achieving 100% internal quantum efficiency (IQE) with associated external quantum efficiencies (EQEs) in OLED devices as high as 21-37% have been reported.[7]

Despite the stellar efficiencies of TADF OLED devices, a truly price-competitive device for lighting has to possess both a simplified architecture and fabrication techniques. The vast majority of TADF OLEDs reported so far have employed a multi-layered device architecture and these layers were deposited by costly vacuum deposition.[8] Solution-processed light-emitting electrochemical cells (LEECs) represent an alternative light-generation technology that enjoys a much simpler device architecture and fabrication process than the OLED analogues.[9] Similar to OLED emitter history, LEEC emitter design has up until very recently been focused mostly on cationic iridium complexes.[9b, 9c, 10] Aside from the use of iridium, a

weakness of LEEC technology to date has been the near complete absence of deep blue emitters.[11]

There exist only a handful of reports of LEECs employing charged small molecule organic emitters, all of which are fluorophores.[9a, 12] We recently reported the first example of a charged purely organic TADF emitters designed for LEECs, which emitted green light thanks to the 4,5-dicarbazolylphthalonitrile luminophore employed.[13] In this study we report deep blue TADF emitters, **imCzDPS** and **imDPADPS** (Figure **1**) and their use in LEECs. The colour of the emission is among the bluest reported so far for this class of devices.

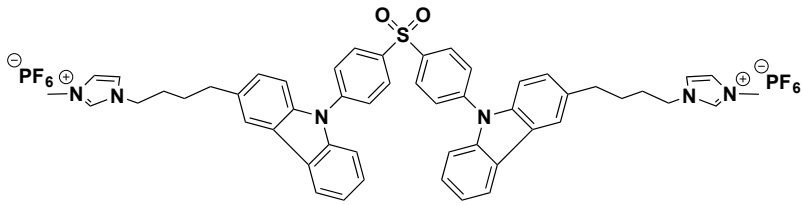

imCzDPS

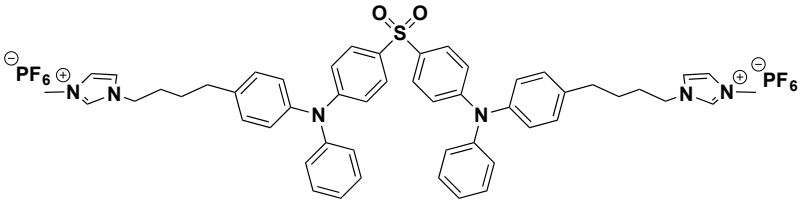

imDPADPS

Figure **1**. Chemical structures of charged emitters **imCzDPS** and **imDPADPS**.

Synthesis

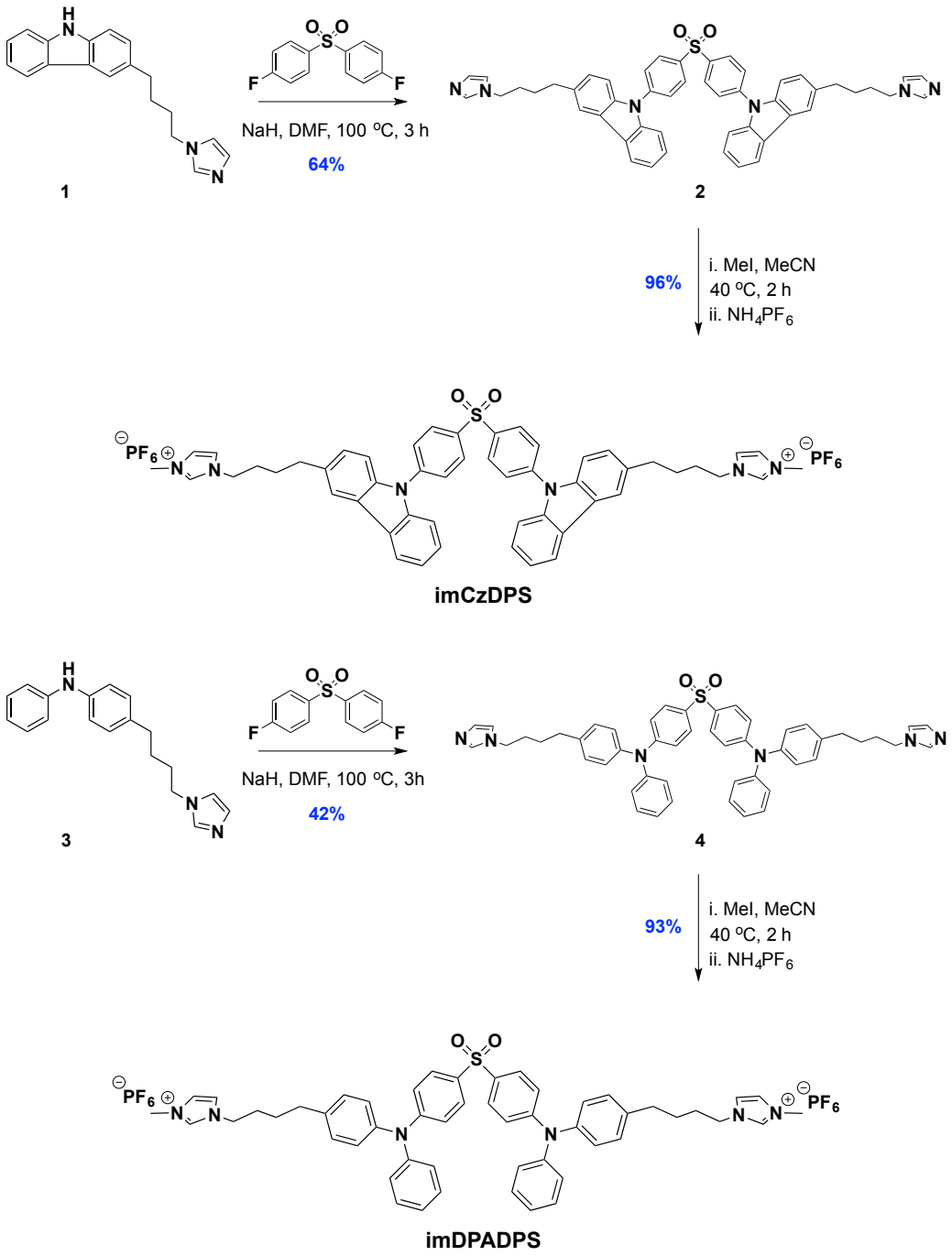

Scheme **1**. Synthetic routes for the **imCzDPS** and **imDPADPS**.

Scheme **1** outlines the synthesis of **imCzDPS** and **imDPADPS**. Two charged imidazolium groups are tethered to the central luminophore through a butylene tether in a similar fashion to our original study.[13] In the current study, a diphenylsulfone (DPS) acceptor was employed as it is a significantly weaker acceptor than the phthalonitrile group, which should lead to a further blue-shift in the emission. A

number of DPS-based TADF emitters have been employed to give very efficient blue (λ_{EL} < 500 nm) OLED devices with EQEs up to 19.8%.[14] Nucleophilic aromatic substitution of 4,4'-difluorodiphenylsulfone with **1** or **3** at 100 °C in dry DMF afforded **2** and **4**, respectively, in moderate yield. Emitters **imCzDPS** and **imDPADPS** were obtained in excellent yield following methylation and anion metathesis. Their identity and purity were established by ^{1}H and ^{13}C NMR, ESI-HRMS and melting point analyses.

Optoelectronic Properties

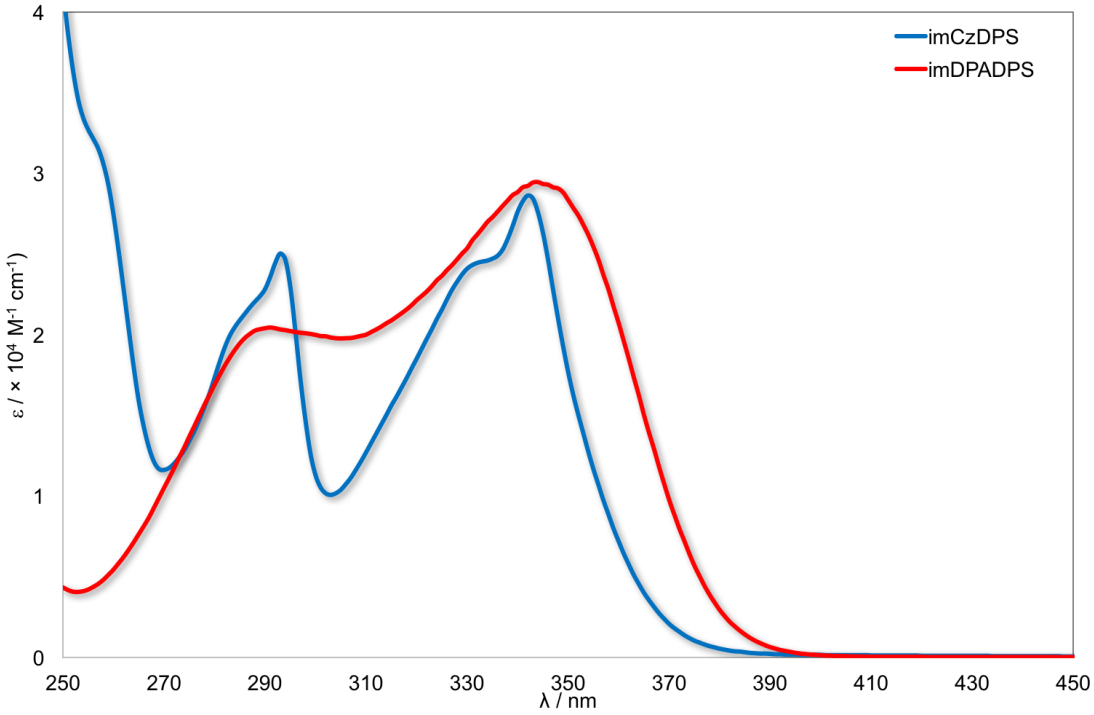

Figure **2**. UV-visible absorption spectra of **imCzDPS** and **imDPADPS** in MeCN.

Table **1**. Absorption and electrochemical data of **imCzDPS** and **imDPADPS**.

Emitter	λ_{abs} [a] / nm, [ε / ×10^4 M^{-1} cm^{-1}]	HOMO[b] / eV	LUMO[c] / eV	E_g [d] / eV
imCzDPS	294 [2.11], 332 [2.23], 343 [2.31]	-5.85	-2.50	3.35

imDPADPS	290 [2.86], 344 [4.13]	-5.52	-2.27	3.25

[a.] in MeCN at 298 K. [b.] in MeCN with 0.1 M [nBu$_4$N]PF$_6$ as the supporting electrolyte and Fc/Fc$^+$ as the internal reference. The HOMO energies were calculated using the equation $E_{HOMO} = -(E^{ox}_{pa} + 4.8)$ eV, where E^{ox}_{pa} is the anodic peak potential.[15] [c.] No reduction processes were observed within the solvent electrochemical window and LUMO levels are inferred from the HOMO energies and bang gap, E_g. [d.] E_g estimated from absorption onset defined as the wavelength at 10% absorbance of the lowest-energy absorption band.

The absorption spectra for **imCzDPS** and **imDPADPS** are shown in Figure **2** and the absorption and electrochemistry data summarized in Table **1** (Figure **S13** shows the corresponding cyclic voltammograms). The absorption bands at ca. 340 nm are assigned to charge-transfer (CT) transitions. The absorption of the CT band in **imDPADPS** is slightly red-shifted compared to that of **imCzDPS** due to stronger donor strength of diphenylamine compared with carbazole.[16] In the cyclic voltammograms (CVs) only oxidation processes were observed within the solvent window, which were assigned to oxidation of the donor groups. The stronger donor strength of the diphenylamine in **imDPADPS** is reflected in its HOMO energy, which is 330 meV higher than that of **imCzDPS**. The oxidation processes for both **imCzDPS** and **imDPADPS** are unsurprisingly irreversible, given the previously reported electrochemical irreversibilities of the carbazole[17] and diphenylamine[18] moieties. The LUMO energies were inferred from the optical band gap, E_g, estimated from the absorption onset and the HOMO energies. The compound **imCzDPS** possessed a modestly larger band gap of 3.35 eV compared to 3.25 eV for **imDPADPS**.

Photophysical Properties

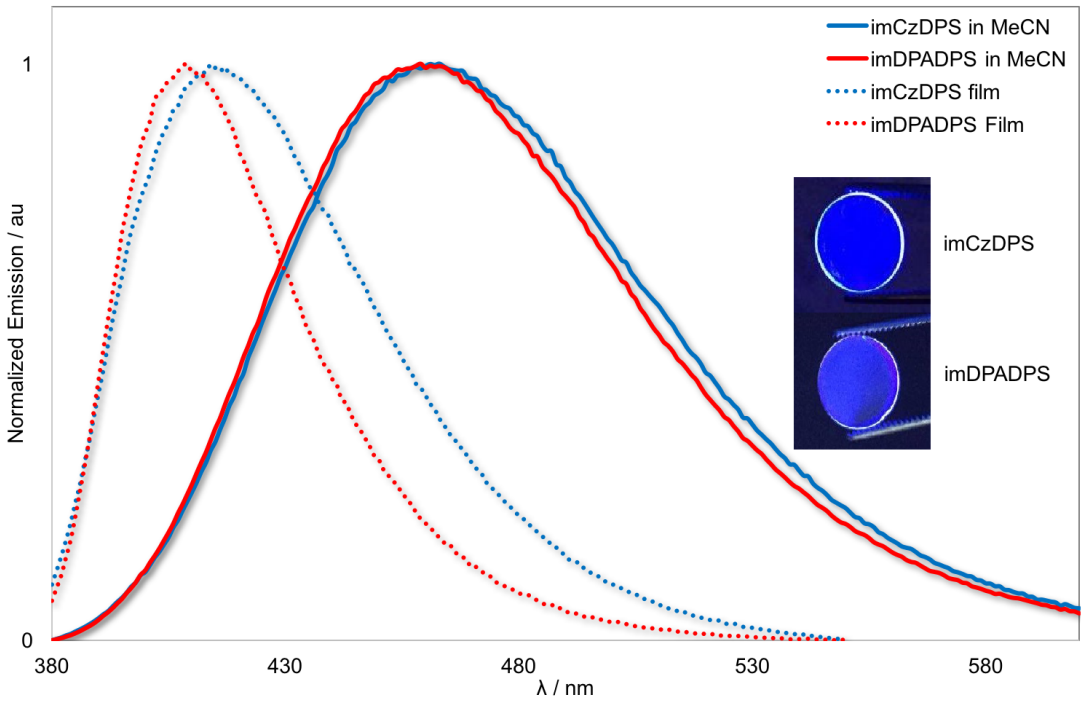

Figure **3**. Emission profiles of **imCzDPS** and **imDPADPS** in degassed MeCN solutions and as doped thin films (5 wt% in PMMA). Inset shows the emission of the doped thin films.

Table **2**. Summary of solution and solid-state photophysical data of **imCzDPS** and **imDPADPS** at 298 K

Emitter	MeCN				5 wt% PMMA[a]			
	λ_{em}[b] / nm	Φ_{PL}[c] / %	τ_p[d] / ns	τ_d[e] / μs	λ_{em}[b] / nm	Φ_{PL}[f] / %	τ_p[d] / ns	τ_d[e] / μs
imCzDPS	463 (93)	54.5 (34.3)	12.2	158	414 (62)	44.1 (46.1)	6.6	48
imDPADPS	459 (92)	63.5 (51.3)	8.9	1621	409 (46)	49.3 (48.3)	3.1	116

[a.] 5 wt% of emitter doped in PMMA spin-coated on quartz from chlorobenzene

solution. [b.] Emission maximum and full-width-at-half-maximum (FWHM) in parentheses. [c.] Φ_{PL} under N_2 were determined using 0.5 M quinine sulfate in H_2SO_4 (aq) as the reference (Φ_r: 54.6%)[19]; Φ_{PL} in air in parentheses. [d] The prompt component of the emission lifetime, τ_p, was measured using Time-Correlated Single Photon Counting (TCSPC) with a time window of 50 ns. [e] The delayed component of the emission lifetime, τ_d, was measured using Multi-Channel Scaling (MCS) with a time window of 1-10 ms. [f] Doped thin film Φ_{PL} values were measured using an integrating sphere under N_2; Φ_{PL} in air in parentheses.

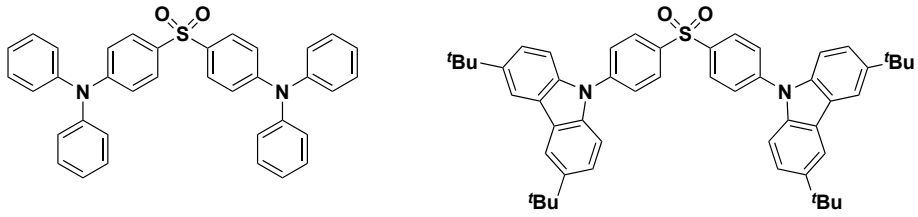

DPADPS tCzDPS

Figure **4**. Reference emitters **DPADPS** and **tCzDPS**.[14a]

The solution-state photophysical properties of **imCzDPS** and **imDPADPS** were assessed in both aerated and degassed MeCN. The solid-state photophysical properties were determined in both neat films and in films consistuted of 5 wt% emitter doped into an inert poly(methylmethacrylate), PMMA matrix. The emission spectra in MeCN and doped thin films are shown in Figure **3** while those in neat films are shown in Figure **4**. The data is summarized in Table **2**. In MeCN, both compounds emit in the blue with near identical emission maxima and FWHM. The photoluminescence quantum yields, Φ_{PL}, are high with **imDPADPS** slightly brighter (63.5%) than **imCzADPS** (54.4%). The emission of the emitters display oxygen sensitivity, with observed decreases in Φ_{PL}, a hallmark of TADF behaviour and

evidence of an accessible triplet state. Both compounds display biexponential emission decay kinetics consisting of a short prompt fluorescence, τ_p, in the nanosecond regime and a longer delayed fluorescence, τ_d, in sub-millisecond to millisecond regime. This decay behaviour is typical of TADF emitters.[20] When doped in PMMA, **imCzDPS** and **imDPADPS** exhibited very deep-blue structureless emission with λ_{max} of 414 nm and 409 nm, respectively, which are blue-shifted by 514 cm^{-1} (9 nm) and 697 cm^{-1} (12 nm), respectively, compared with reference TADF emitters **tCzDPS** and **DPADPS** (Figure **4**) doped in DPEPO.[14a] The small blue-shift in our case is likely due to PMMA being a less polar matrix than DPEPO. The emission lifetimes of the delayed component (48 μs for **imCzDPS** and 118 μs for **imDPADPS**) are also much shorter than **tCzDPS** and **DPADPS** (540 μs and 850 μs, respectively), which illustrates how sensitive the photophysical properties are to decoration about the donor and matrix choice. The red-shifted emission in MeCN is due to the positive solvatochromism of the donor-acceptor molecular architecture in the polar solvent. The prototype emitters **DPADPS** and **tCzDPS** demonstrated emission maxima at 402 nm and 404 nm, respectively, in toluene, with comparable Φ_{PL} (57% and 69%, respectively) to **imCzDPS** and **imDPADPS** in MeCN. The blue-shifted nature of these compounds in PhMe is due to the measurements being conducted in this less polar solvent. Thin film Φ_{PL} values are modestly lower (44% and 49% for **imCzDPS** and **imDPADPS**, respectively) than those in MeCN and show negligible sensitivity to oxygen due to the low oxygen permeability of the PMMA host.[13, 21] As neat films the emission maxima of 440 nm and 428 nm for **imCzDPS** and **imDPADPS**, respectively, are moderately red-shifted by 1427 cm^{-1} (26 nm) and 1085 cm^{-1} (19 nm) with respect to those found for the PMMA doped thin films. Gratifyingly, their Φ_{PL} values of 44 and 61% for **imCzDPS** and **imDPADPS**,

respectively, are very similar to those found for the doped thin films. Both compounds show prompt and delayed emission lifetimes, with the delayed component an order of magnitude shorter than those found in MeCN.

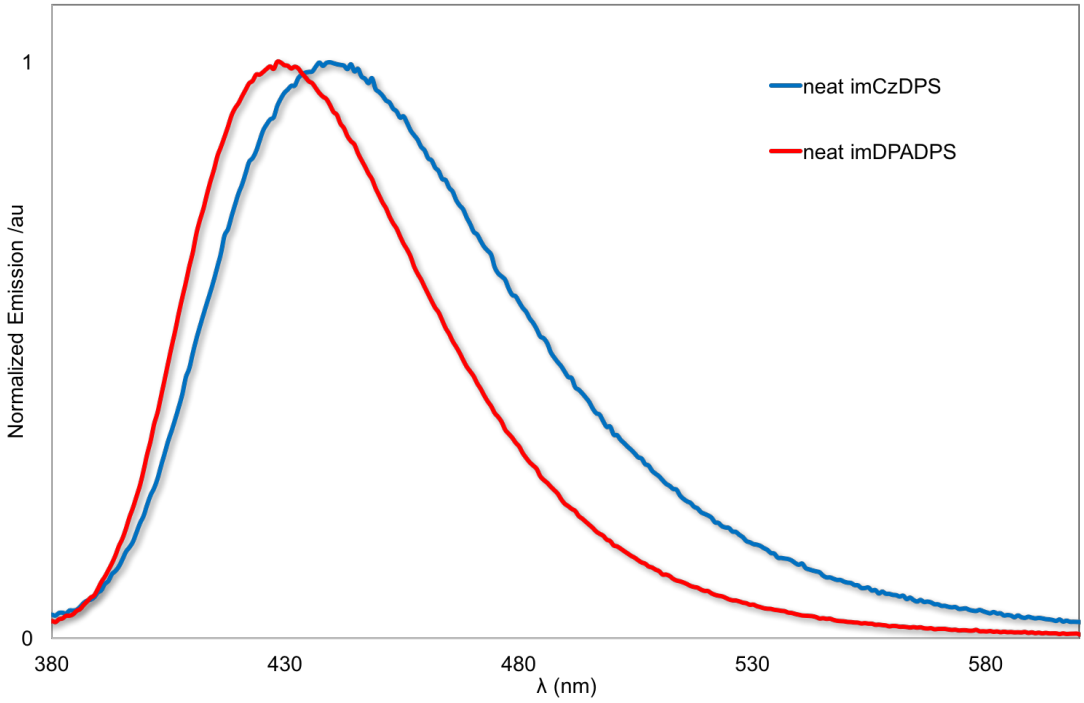

Figure **5**. Emission spectra of **imCzDPS** and **imDPADPS** as neat films.

Light-emitting electrochemical cells

LEECs were prepared by solution deposition of an 80 nm layer of PEDOT:PSS (poly(3,4-ethylenedioxythiophene): poly(styrenesulfonate)) on pre-patternered ITO-coated substrates followed by spin-coating the emissive layer from of a 20 mg mL^{-1} MeCN solution of **imCzDPS** or **imDPADPS**. An aluminum top metal electrode was thermally evaporated onto the devices in a high-vacuum chamber integrated into an inert atmosphere glovebox. Devices were driven by applying a pulsed current at a frequency of 1000 Hz and a duty cycle of 50%. This biasing mode allows a better stabilization of the LEECs operation by reducing the turn-on time without compromising the device lifetime.[22]

Using this approach, when applying an average current density of 200 A m^{-2} we observed electroluminescence from the device employing **imCzDPS** in a single layer LEEC (Figure **6**). Surprisingly, under the same operation conditions no emission from the device with **imDPADPS** could be observed.

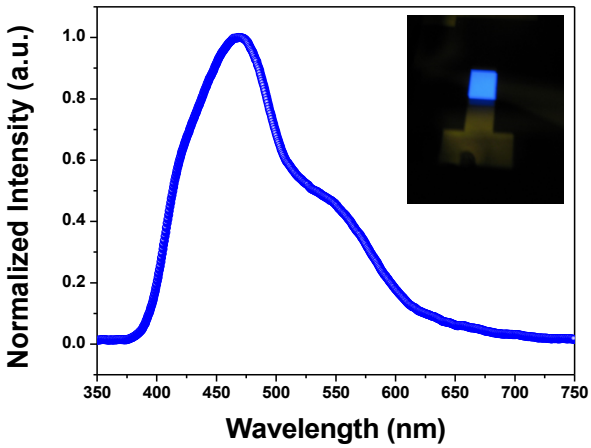

Figure **6**. Normalized EL spectrum of LEEC with **imCzDPS**, operated by applying an average current density of 200 A m^{-2} in a pulsed mode using a block wave with a frequency of 1000 Hz and a duty cycle of 50 %.

The electroluminescence spectrum of this LEEC shows a maximum at 470 nm and a shoulder around 550 nm. The device shows a deep blue emission with CIE coordinates of (0.208, 0.250), results that indicate the potential of TADF small molecules for developing white light-emitting devices. A slight shift of around 30 nm for the emitter band in the EL compared to the PL may suggest the presence of emissive aggregates while the shoulder is likely related to the emission of new

molecules/ species oxidized as a result of the irreversible oxidation process observed for **imCzDPS**.

To obtain more insight into the operation of the devices, the luminance and voltage needed to sustain the average current density applied were monitored over time. The luminance, the average voltage and external quantum efficiency (EQE) data are reported in Figure **7**.

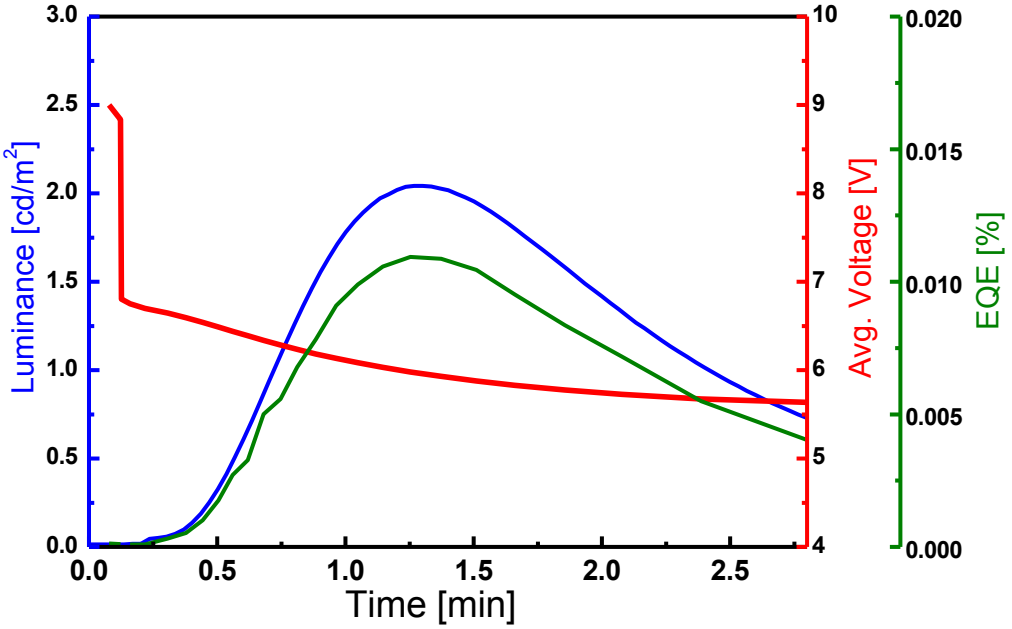

Figure **7**. Luminance, average voltage and external quantum efficiency for the LEEC using **imCzDPS** as the emissive material, operated by applying an average current density of 200 A m^{-2} in a pulsed mode using a block wave with a frequency of 1000 Hz and a duty cycle of 50 %.

The driving voltage decreased upon application of the pulsed current bias indicating that the devices do operate as LEECs. In LEECs the injection barrier for

electrons and holes is reduced by the separation of the ions in the light-emitting layer to the electrode interfaces. Upon injecting electronic carriers, this leads to the formation of doped regions with lower resistance than the intrinsic film, which explains the reduction in driving voltage observed in our devices.[23] The luminance slowly increased over time, indicating that the ionic movement is not very fast or that the electronic carrier injection is slow due to a large energy barrier at one of the interfaces. The luminance levels obtained are modest, yet are deep blue, which is a region of the visible spectrum in which the human eye is not very sensitive. Among the LEECs based on organic small molecules,[9a, 12] the **imCzDPS** device is among the bluest. Previous reports of deep-blue LEEC devices include ionic bis(2-naphthyl)fluorene[12a] and bis(1-pyrenyl)fluorene[24] fluorophores which show λ_{EL} at 432 nm and 454 nm, respectively, and corresponding CIE coordinates of (0.15, 0.09) and (0.16, 0.22), respectively. The LEEC employing bis(2-naphthyl)fluorene gave a current efficiency of 0.15 cd A^{-1} while the LEEC using bis(1-pyrenyl)fluorene gave a current efficiency of 0.14 cd A^{-1}. An ionic terfluorene[25] emitter also gave a deep-blue LEEC device with λ_{EL} and CIE at 423 nm and (0.15, 0.12), respectively with an EQE of 1.14%. Each of these emitters had very high Φ_{PL} in solution (77-100%) and all showed highly reversible oxidation waves, yet their reduction waves were either undetectable or irreversible. Therefore, the poorer efficiencies of the LEEC devices in this study are attributed to the electrochemical instability of the emitter, as evidenced by the appearance of additional lower energy peak in EL spectrum (Figure **6**). Nevertheless, the distinct feature of this study is the ability to recruit dark triplet excitons in the device, which is not possible with the charged fluorophores reported in the literature.

Conclusions

In this study, two TADF emitters with tethered charged groups, **imCzDPS** and **imDPADPS**, designed for LEECs were synthesized and fully characterized. The TADF nature of these emitters in both MeCN and as doped PMMA films is supported by the presence of microsecond delayed component of the emission decay and enhancement in the photoluminescence quantum yields after removal of oxygen from the medium. Despite strong emission in the deep blue region (414 and 409 nm with Φ_{PL} 44% and 49% in 5 wt% PMMA for **imCzDPS** and **imDPADPS**, respectively), only the LEEC with **imCzDPS** produced light, albeit deep blue emission with a very poor efficiency, which was attributed to the electrochemical instability of the emitter.

Supporting Information. Experimental section. ^{1}H NMR spectra for all compounds. Cyclic voltammograms of **imCzDPS** and **imDPADPS**.

Acknowledgements

We acknowledge the University of St Andrews for financial support. We thank the EPSRC UK National Mass Spectrometry Facility at Swansea University for analytical services. We acknowledge financial support from the European Union H2020 project INFORM (grant 675867), the Spanish Ministry of Economy and Competitiveness (MINECO) via the Unidad de Excelencia María de Maeztu MDM-2015-0538, MAT2014-55200 and the Generalitat Valenciana (Prometeo/2016/135). MLP acknowledges support from a Grisolia grant (GRISOLIA/2015/A/146).

References

(1). H. Sasabe and J. Kido, *Eur. J. Org. Chem.*, 2013, **2013**, 7653-7663.
(2). M. A. Baldo, D. F. O'Brien, Y. You, A. Shoustikov, S. Sibley, M. E. Thompson and S. R. Forrest, *Nature*, 1998, **395**, 151-154.
(3). (a) I. Kondrasenko, Z. H. Tsai, K. Y. Chung, Y. T. Chen, Y. Y. Ershova, A. Domenech-Carbo, W. Y. Hung, P. T. Chou, A. J. Karttunen and I. O. Koshevoy, *ACS Appl Mater Interfaces*, 2016, **8**, 10968-10976; (b) B. Zhao, T. Zhang, B. Chu, W. Li, Z. Su, H. Wu, X. Yan, F. Jin, Y. Gao and C. Liu, *Sci Rep*, 2015, **5**, 10697.
(4). (a) B. Minaev, G. Baryshnikov and H. Agren, *Phys Chem Chem Phys*, 2014, **16**, 1719-1758; (b) Y. You and W. Nam, *Chem. Soc. Rev.*, 2012, **41**, 7061-7084.
(5). (a) L. Bergmann, D. M. Zink, S. Bräse, T. Baumann and D. Volz, *Top. Curr. Chem.*, 2016, **374**, 1-39; (b) C. Adachi, *Jpn. J. Appl. Phys.*, 2014, **53**, 060101.
(6). (a) Y. Tao, K. Yuan, T. Chen, P. Xu, H. Li, R. Chen, C. Zheng, L. Zhang and W. Huang, *Adv. Mater.*, 2014, **26**, 7931-7958; (b) H. Uoyama, K. Goushi, K. Shizu, H. Nomura and C. Adachi, *Nature*, 2012, **492**, 234-238.
(7). (a) M. Taneda, K. Shizu, H. Tanaka and C. Adachi, *Chem. Commun.*, 2015, **51**, 5028-5031; (b) H. Kaji, H. Suzuki, T. Fukushima, K. Shizu, K. Suzuki, S. Kubo, T. Komino, H. Oiwa, F. Suzuki, A. Wakamiya, Y. Murata and C. Adachi, *Nat Commun*, 2015, **6**, 8476; (c) T.-A. Lin, T. Chatterjee, W.-L. Tsai, W.-K. Lee, M.-J. Wu, M. Jiao, K.-C. Pan, C.-L. Yi, C.-L. Chung, K.-T. Wong and C.-C. Wu, *Adv. Mater.*, 2016, **28**, 6976-6983.
(8). D. Volz, M. Wallesch, C. Fléchon, M. Danz, A. Verma, J. M. Navarro, D. M. Zink, S. Bräse and T. Baumann, *Green Chem.*, 2015, **17**, 1988-2011.
(9). (a) A. Pertegás, D. Tordera, J. J. Serrano-Pérez, E. Ortí and H. J. Bolink, *J. Am. Chem. Soc.*, 2013, **135**, 18008-18011; (b) A. F. Henwood and E. Zysman-Colman, *Top. Curr. Chem.*, 2016, **374**, 1-41; (c) R. D. Costa, E. Ortí, H. J. Bolink, F. Monti, G. Accorsi and N. Armaroli, *Angew. Chem. Int. Ed.*, 2012, **51**, 8178-8211.
(10). (a) J. D. Slinker, J. Rivnay, J. S. Moskowitz, J. B. Parker, S. Bernhard, H. D. Abruña and G. G. Malliaras, *J. Mater. Chem.*, 2007, **17**, 2976-2988; (b) H.-C. Su, H.-F. Chen, P.-H. Chen, S.-W. Lin, C.-T. Liao and K.-T. Wong, *J. Mater. Chem.*, 2012, **22**, 22998-23004; (c) T. Hu, L. He, L. Duan and Y. Qiu, *J. Mater. Chem.*, 2012, **22**, 4206-4215.
(11). (a) D. Rota Martir, A. K. Bansal, V. Di Mascio, D. B. Cordes, A. F. Henwood, A. Slawin, P. Kamer, L. Martinez-Sarti, A. Pertegas, H. J. Bolink, I. Samuel and E. Zysman-Colman, *Inorganic Chemistry Frontiers*, 2015, **ASAP**, DOI: 10.1039/C1035QI00177C; (b) A. F. Henwood, A. K. Bansal, D. B. Cordes, A. M. Z. Slawin, I. D. W. Samuel and E. Zysman-Colman, *J. Mater. Chem. C*, 2016, **4**, 3726-3737; (c) L. He, L. Duan, J. Qiao, R. Wang, P. Wei, L. Wang and Y. Qiu, *Adv. Funct. Mater.*, 2008, **18**, 2123-2131; (d) S. B. Meier, W. Sarfert, J. M. Junquera-Hernández, M. Delgado, D. Tordera, E. Ortí, H. J. Bolink, F. Kessler, R. Scopelliti, M. Grätzel, M. K. Nazeeruddin and E. Baranoff, *J. Mater. Chem. C*, 2013, **1**, 58; (e) S. Evariste, M. Sandroni, T. W. Rees, C. Roldan-Carmona, L. Gil-Escrig, H. J. Bolink, E. Baranoff and E. Zysman-Colman, *J. Mater. Chem. C*, 2014, **2**, 5793-5804; (f) C. D. Sunesh, K. Shanmugasundaram, M. S. Subeesh, R. K. Chitumalla, J. Jang and Y. Choe, *ACS Appl Mater Interfaces*, 2015, **7**, 7741-7751.
(12). (a) K. Shanmugasundaram, M. S. Subeesh, C. D. Sunesh and Y. Choe, *RSC Adv.*, 2016, **6**, 28912-28918; (b) M. S. Subeesh, K. Shanmugasundaram, C. D. Sunesh, T. P. Nguyen and Y. Choe, *J. Phys. Chem. C*, 2015, **119**, 23676-23684; (c) M. S. Subeesh, K. Shanmugasundaram, C. D. Sunesh, R. K. Chitumalla, J. Jang and Y. Choe, *J. Phys. Chem. C*, 2016, **120**, 12207-12217; (d) K. Shanmugasundaram, M. S. Subeesh, C. D. Sunesh, R. K. Chitumalla, J. Jang and Y. Choe, *J. Phys. Chem. C*, 2016, **120**, 20247-20253.
(13). M. Y. Wong, G. J. Hedley, G. Xie, L. S. Kölln, I. D. W. Samuel, A. Pertegás, H. J. Bolink and E. Zysman-Colman, *Chem. Mater.*, 2015, **27**, 6535-6542.

(14). (a) Q. Zhang, J. Li, K. Shizu, S. Huang, S. Hirata, H. Miyazaki and C. Adachi, *J Am Chem Soc*, 2012, **134**, 14706-14709; (b) S. Wu, M. Aonuma, Q. Zhang, S. Huang, T. Nakagawa, K. Kuwabara and C. Adachi, *J. Mater. Chem. C*, 2014, **2**, 421-424; (c) Q. Zhang, B. Li, S. Huang, H. Nomura, H. Tanaka and C. Adachi, *Nature Photonics*, 2014, **8**, 326-332; (d) I. Lee and J. Y. Lee, *Org. Electron.*, 2016, **29**, 160-164.
(15). C. M. Cardona, W. Li, A. E. Kaifer, D. Stockdale and G. C. Bazan, *Adv. Mater.*, 2011, **23**, 2367-2371.
(16). H. Wang, L. Xie, Q. Peng, L. Meng, Y. Wang, Y. Yi and P. Wang, *Adv. Mater.*, 2014, **26**, 5198-5204.
(17). A. Tomkeviciene, J. V. Grazulevicius, D. Volyniuk, V. Jankauskas and G. Sini, *Phys Chem Chem Phys*, 2014, **16**, 13932-13942.
(18). L. Xu, H. Zhu, G. Long, J. Zhao, D. Li, R. Ganguly, Y. Li, Q.-H. Xu and Q. Zhang, *J. Mater. Chem. C*, 2015, **3**, 9191-9196.
(19). W. H. Melhuish, *J. Phys. Chem.*, 1961, **65**, 229-235.
(20). (a) J. Lee, K. Shizu, H. Tanaka, H. Nomura, T. Yasuda and C. Adachi, *J. Mater. Chem. C*, 2013, **1**, 4599; (b) H. Tanaka, K. Shizu, H. Miyazaki and C. Adachi, *Chem. Commun.*, 2012, **48**, 11392-11394; (c) Y. J. Cho, K. S. Yook and J. Y. Lee, *Adv. Mater.*, 2014, **26**, 6642-6646; (d) P. Data, P. Pander, M. Okazaki, Y. Takeda, S. Minakata and A. P. Monkman, *Angew. Chem. Int. Ed.*, 2016, **55**, 5739-5744; (e) K. Suzuki, S. Kubo, K. Shizu, T. Fukushima, A. Wakamiya, Y. Murata, C. Adachi and H. Kaji, *Angew Chem Int Ed Engl*, 2015, **54**, 15231-15235.
(21). P. L. Dos Santos, J. S. Ward, M. R. Bryce and A. P. Monkman, *J Phys Chem Lett*, 2016, **7**, 3341-3346.
(22). D. Tordera, S. Meier, M. Lenes, R. D. Costa, E. Ortí, W. Sarfert and H. J. Bolink, *Adv. Mater.*, 2012, **24**, 897-900.
(23). (a) S. van Reenen, P. Matyba, A. Dzwilewski, R. A. J. Janssen, L. Edman and M. Kemerink, *J. Am. Chem. Soc.*, 2010, **132**, 13776-13781; (b) D. B. Rodovsky, O. G. Reid, L. S. C. Pingree and D. S. Ginger, *ACS Nano*, 2010, **4**, 2673-2680; (c) M. Lenes, G. Garcia-Belmonte, D. Tordera, A. Pertegás, J. Bisquert and H. J. Bolink, *Adv. Funct. Mater.*, 2011, **21**, 1581-1586.
(24). K. Shanmugasundaram, M. S. Subeesh, C. D. Sunesh, R. K. Chitumalla, J. Jang and Y. Choe, *Org. Electron.*, 2015, **24**, 297-302.
(25). H.-F. Chen, C.-T. Liao, T.-C. Chen, H.-C. Su, K.-T. Wong and T.-F. Guo, *J. Mater. Chem.*, 2011, **21**, 4175.

TOC graphic